Journal of Visualized Experiments

Characterization of SiN Integrated Optical Phased Arrays on a Wafer-Scale Test Station

--Manuscript Draft--

Article Type:	Invited Methods Article - JoVE Produced Video
Manuscript Number:	JoVE60269R1
Full Title:	Characterization of SiN Integrated Optical Phased Arrays on a Wafer-Scale Test Station
Section/Category:	JoVE Engineering
Keywords:	LIDAR; solid state; silicon photonics; 3D imaging; integrated optics; beam scanning; beam steering; self driving; optical characterisation
Corresponding Author:	Daivid Fowler CEA-LETI Grenoble, Isère FRANCE
Corresponding Author's Institution:	CEA-LETI
Corresponding Author E-Mail:	Daivid.FOWLER@cea.fr
Order of Authors:	Nicola A. Tyler
	Sylvain Guerber
	Daivid Fowler
	Stephane Malhouitre
	Stephanie Garcia
	Philippe Grosse
	Bertrand Szelag
Additional Information:	
Question	**Response**
Please indicate whether this article will be Standard Access or Open Access.	Open Access (US$4,200)
Please indicate the **city, state/province, and country** where this article will be **filmed**. Please do not use abbreviations.	Grenoble, Isère, France

TITLE:

Characterization of SiN Integrated Optical Phased Arrays on a Wafer-Scale Test Station

AUTHORS AND AFFILIATIONS:

Nicola A. Tyler, Sylvain Guerber, Daivid Fowler, Stephane Malhouitre, Stephanie Garcia, Philippe Grosse, and Bertrand Szelag

University Grenoble Alpes and CEA, LETI, Minatec Campus, Grenoble Cedex, France

Email addresses of co-authors:
Nicola A. Tyler: nicola.a.tyler@gmail.com
Sylvain Guerber: sylvain.guerber@cea.fr
Stephane Malhouitre: stephane.malhouitre@cea.fr
Stephanie Garcia: stephanie.garcia@cea.fr
Philippe Grosse: philippe.grosse@cea.fr
Bertrand Szelag: Bertrand.Szelag@cea.fr

Corresponding author:
Daivid Fowler: Daivid.fowler@cea.fr

KEYWORDS:

Optical phased arrays, integrated photonics, SiN, silicon photonics, beam steering, LIDAR, two-dimensions, single wavelength

SUMMARY:

Here, we describe the operation of a SiN integrated photonic circuit containing optical phased arrays. The circuits are used to emit low divergence laser beams in the near infrared and steer them in two dimensions.

ABSTRACT:

Optical phased arrays (OPAs) can produce low-divergence laser beams and can be used to control the emission angle electronically without the need for moving mechanical parts. This technology is particularly useful for beam steering applications. Here, we focus on OPAs integrated into SiN photonic circuits for a wavelength in the near infrared. A characterization method of such circuits is presented, which allows the output beam of integrated OPAs to be shaped and steered. Furthermore, using a wafer-scale characterization setup, several devices can easily be tested across multiple dies on a wafer. In this way, fabrication variations can be studied, and high-performance devices identified. Typical images of OPA beams are shown, including beams emitted from OPAs with and without a uniform waveguide length, and with varying numbers of channels. In addition, the evolution of output beams during the phase optimization process and beam steering in two dimensions is presented. Finally, a study of the variation in the beam divergence of identical devices is performed with respect to their position on the wafer.

INTRODUCTION:

Optical phased arrays (OPAs) are advantageous due to their ability to shape and steer optical beams nonmechanically – this is useful in a broad range of technological applications such as light detection and ranging (LIDAR), free space communication and holographic displays[1]. The integration of OPAs in photonic circuits is of particular interest, as it provides a low cost solution for their fabrication with a small physical footprint. Integrated OPAs have been successfully demonstrated using a number of different material systems including InP, AlGaAs and silicon[2-4]. Of these systems, silicon photonics is perhaps the most convenient, due to its high refractive index contrast and compatibility with CMOS[5]. Indeed, OPA circuits have been extensively demonstrated in the silicon-on-insulator platform[6-10]; however, the application of these circuits is limited both by the wavelength transparency window of silicon and the high nonlinear losses, which lead to a limit on the available output optical power. We focus instead on OPAs integrated in SiN, a material with similar properties to silicon in terms of CMOS capability and footprint size[11,12]. In contrast to silicon however, SiN is expected to be suitable for a larger range of applications since the transparency window is broader, down to at least 500 nm, and thanks to the possibly high optical power thanks to the relatively low nonlinear losses.

The principals of OPA integration have recently been demonstrated using SiN[8,13,14]. Here, we will extend these principals to demonstrate a method of characterizing and operating integrated OPAs for two dimensional beam steering. In comparison to previous demonstrations of beam steering in two dimensions that rely on the tuning of the wavelength[6], our circuit can operate at a single wavelength. We first provide a brief overview of the operating principles behind OPAs. This is followed by an introduction to the circuits used in this work. Finally, the characterization method is described and typical images of OPA output beams presented and discussed.

OPAs are composed of an array of closely spaced emitters that can be addressed individually to control the optical phase. If a linear phase relationship exists across the emitter array, the interference pattern in the far field yields several clearly separated maxima - similar to the principles of multi-slit interference. By controlling the magnitude of the phase difference, the position of the maxima can be adjusted, and hence, beam steering performed. In integrated OPAs, emitters consist of closely spaced diffraction gratings where the light is scattered and emitted out of the chip plane. A schematic illustration of an integrated OPA device is shown in **Figure 1A,B**. Light is coupled into the chip, in this case via an optical fiber, and is then divided into multiple channels, each containing an integrated phase shifter. At the other end of the optical circuit, the waveguides terminate in gratings and combine to form the OPA. The resulting output beam is comprised of multiple interference maxima, the brightest of which is referred to as the fundamental lobe and is the one most often used in beam steering applications. The emission direction of the fundamental lobe is defined by the two azimuthal angles to the orthogonal projection of the chip plane, ϕ and θ, perpendicular and parallel to the orientation of the grating respectively. In this document, ϕ and θ will be referred to as the 'perpendicular' and 'parallel' emission angles, respectively. The perpendicular angle ϕ is determined by the phase difference between the OPA channels, and the parallel angle θ depends on the period of the output gratings.

Our integrated circuits are fabricated using Si_3N_4 waveguides with a cross section of 600 x 300 nm^2, a design that was optimized for the fundamental transverse electric polarization mode of light at a wavelength of 905 nm. Underneath the waveguides lies a 2.5 µm SiO_2 buffer layer on top of a silicon wafer. The thermal phase shifters were made from a 10(100) nm thick Ti(TiN) layer used to form 500 µm long and 2 µm wide resistive wires. In our circuits, an electric power of 90 mW is required to achieve a phase shift of π. The OPA output gratings consist of 750 fully etched periods with a nominal filling factor of 0.5 and a grating period between 670 nm and 700 nm. Further information on the platform design and fabrication is given in Tyler et al.[15,16].

In this work, two different types of circuits are characterized, a passive circuit without phase shifting capabilities, and a more complex circuit, designed to perform beam steering in two dimensions. The two dimensional beam steering circuit is shown in **Figure 2**. **Figure 2A** contains a schematic of the circuit and **Figure 2B** shows a microscope image of the fabricated device. The light enters the circuit at the input grating. It then reaches a switching network where it can be routed selectively towards one of four sub-circuits. Each sub-circuit splits the light into four channels using multimode interference devices (MMI). The channels each contain a thermal phase shifter and form an OPA at the end of the circuit. The four OPAs originating from the four sub-circuits each comprise a different grating period between 670 nm and 700 nm. These periods correspond to azimuthal angles parallel to the grating axis, θ, between 7° and 10°. A more detailed description on the circuit can be found in Tyler et al.[16].

The presented characterization setup is based on an automated probing station capable of performing a series of measurements on many circuits across a whole wafer. This enables study of the performance variation relative to the position on the wafer and to select the devices with the optimum properties. However, the use of a prober station implies some physical constraints to the OPA characterization scheme due to the relatively small available space above the wafer. The characterization of optical phased arrays requires imaging the OPA output in the far field, which can be performed in a number of ways. For example, a series of lenses may be used in a Fourier imaging system[6] or the farfield image formed on a Lambertian surface may be viewed in either reflection or transmission. For our system, we chose what we considered to be the simplest and most compact solution of placing a large surface 35 mm x 28 mm CMOS sensor without lenses placed approximately 50 mm above the wafer surface. Despite the increased cost of such a large CCD sensor, this solution allows a sufficient field of view without the use of lenses.

PROTOCOL:

1. Preparations

1.1. Prepare the following experimental setup (Figure 4).

1.1.1. Use a computer.

1.1.2. Use a continuous wave fiber coupled laser source. Depending on the circuit losses, 1 mW power suffices. In the presented characterization setup, the laser source is at a wavelength of

905 nm.

1.1.3. Use a polarization controller adapted for the laser wavelength.

1.1.4. Use a cleaved input fiber to couple light into the input grating coupler of the optical circuit.

1.1.5. Use an electric probe to connect the electronic control board to the electrical contact of the optical circuit.

1.1.6. Use a system capable of controlling the 20 phase modulators of the two dimensional beam steering circuit is required. In the presented characterization setup, this system is a custom electronic board controlled by an Arduino, which is able to apply individually between 0 and 200 mW of electric power at the phase shifters on the optical circuit. A schematic of the electrical circuit is shown in **Figure 3**. For each channel, the circuit contain a DAC (Digital to Analog Converter) that will translate the digital command voltage to an analog voltage that controls the gate of a high-power transistor. The heater is connected to a high-power current source. Therefore, by controlling the gate tension, the current flow in the heater can be adjusted.

1.1.7. Use a bare image sensor to image the far field of the optical output. In the presented characterization setup, the camera is a 35 mm CCD sensor.

1.1.8. Use a optical microscope in order to image the chip for alignment purposes.

1.1.9. Use a 3-axis translation stage and mount to fit a 200 mm wafer. In the presented characterization setup, this stage is a reconfigurable probe system for silicon photonics.

1.2. Equipment assembly

1.2.1. Assemble the equipment according to **Figure 4** and mount the wafer. The distance between wafer and the sensor needs to be chosen small enough to ensure a high-resolution image of the output beam, but large enough to fit at least two interference maxima in order to be able to find the relationship between sensor pixels and output angle as will be explained in section 4 of the protocol.

1.2.2. Ensure that the sensor and the wafer are parallel; otherwise, it may falsify the computation of the pixel/output angle computation. In the presented characterization setup, set the wafer-sensor distance to 5 cm. If a double sensor configuration is used (like the one presented here), ensure that the bare sensor can easily be removed to give access to the optical microscope in order to image the near-field for fiber alignment purposes.

1.2.3. Be sure that the electrical probe, camera and optical fiber are not touching each other.

Connect required elements to a computer. In the presented setup the probe station, the CCD sensor and the electrical circuit for the phase control are driven via a computer and a Python program in order to automate the measurement process.

2. Optical coupling

2.1. Fiber alignment

2.1.1. Using the microscope, start by carefully lowering the fiber until it touches the wafer surface (away from the input grating coupler to avoid damaging it), and then move it up about 20 µm.

2.1.2. When this is done, maximize the light intensity at the output gratings. To do so, start sweeping the fiber position over the OPA input grating coupler. If the camera attached to the microscope is responsive to the laser wavelength (if not use the bare image sensor), and if the fiber and grating coupler are well aligned, light exiting at the OPA output gratings should be visible on the image. An example can be seen in **Figure 5A**.

2.1.3. When light is seen from the OPA antennas, adjust the polarization in order to maximize the light intensity at the output gratings. Be sure to avoid any movement or vibration of the input fiber

2.2. OPA output imaging

2.2.1. Switch to the far-field imaging sensor and improve the image quality: Adjust both the exposure time of the sensor and the laser power in such a way that the OPA output is clearly visible on the camera and the beam does not saturate the sensor. An example image recorded by the sensor is shown in **Figure 5B**.

2.2.2. If necessary, cover the setup so that the background light does not interfere with the image from the OPA beam. Generally, the weaker the background light, the lower the laser power that can be set.

2.2.3. Block the reflections by placing a highly reflecting sheet between the reflection and the camera. Sometimes, reflections originating from the wafer surface reach the sensor area and contaminate the image of the OPA output (reflections can happen at the input grating).

2.2.4. Readjust the polarization of the input light to obtain a clear image.

3. Beam optimization and steering

NOTE: This section describes the operation of the circuit shown in **Figure 2** and how it can be used to perform beam steering in two dimensions.

3.1. Preparations

3.1.1. Connect the electric circuit for the phase control to a multi-channel electric probe.

3.1.2. Using the microscope, connect the pins of the electric probe to the metal contact pads of the optical circuit.

3.1.3. Re-optimize the position of the input fiber.

3.1.4. Switch to the far field sensor and image the output.

3.2. Selection of the parallel emission angle θ using the switching network

3.2.1. Study the ring resonators of the switching network in order to control the emission angle in θ. For this purpose, observe the far field image of the output while varying the voltages applied to the phase shifters at the ring resonators. With the correct voltage applied to each resonator, a different area on the sensor will be illuminated, corresponding to a certain θ value, as shown in **Figure 6B**.

3.2.2. Find the voltages where the rings are on- and off-resonance. For this purpose, an automated script can be used to sweep the resonator voltages and record the intensities on the different θ areas on the sensor. Use found voltages to access the various sub-circuits and to steer the output beam in θ.

3.3. Selection of the orthogonal emission angle ϕ by optimizing the OPA phases

3.3.1. Optimize the OPA phases in order to shape and steer the output beam in ϕ. For this purpose, select a small pixel area (corresponding to the desired ϕ angle) that should be illuminated with a focused output beam.

3.3.2. Maximize the brightness inside the chosen area by running the following the optimization routine.

3.3.2.1. Shift the phase of one of the OPA channels in small increments. After each shift, record the integral of the brightness in the pixel area inside, I_i, and outside, I_o, of the selected area. Calculate the ratio $R = I_i / I_o$. After a full phase shift cycle between 0 and 2π, apply the phase shift with the highest recorded brightness ratio R.

3.3.2.2. Repeat this phase optimization process on the next OPA channel. Different optimization algorithms may be used, such as a hill climbing.

3.3.2.3. Repeat the optimization process by optimizing the phases until the optimization process

is saturated and a focused output beam is visible. Example images of the output beam taken during an optimization process is shown in **Figure 6A**. After 16 optimization rounds, the output beam a focused beam is visible.

NOTE: If some additional unexpected peaks are present, this may be a result of a temporally unstable coupling into the circuit during the optimization process. This may be due to movement of the input fiber and/or an unstable polarization state.

3.3.3. In order to steer the output beam to a different ϕ angle, select a new pixel area and repeat the optimization process.

4. Beam divergence measurements and image analysis

4.1. Image acquisition

4.1.1. Optimize the position of the input fiber. Record the image of the output in the far-field. Make sure that at least two clear interference maxima are visible.

4.1.2. Using the alignment system, move the wafer in order to align the next device to the input fiber. Perform fine alignment by maximizing the output intensity recorded by the camera. Record output image.

4.1.3. Repeat the above step until all devices of interest have been characterized. If the selected optical circuit has the capability of phase adjustment of the OPA channels, perform a phase optimization routine before recording the images.

4.2. Image analysis

4.2.1. Check the recorded images for false data points arising from defective pixels, such as dead or hot pixels. Erase these data points or replace the values by typical values.

4.2.2. Correlate the CCD pixels to OPA output angles ϕ and θ as follows.

4.2.2.1. Calculate the angular distance Δϕ between the interference maxima according to the OPA design using $\Delta\phi = \sin^{-1}(\lambda/d)$ [°], where λ is the wavelength and d is the lateral pitch between the OPA gratings. Fit two Gaussian curves to the two interference maxima and determine the positions of the two centers, P_1 and P_2. Since the distance (in pixels) between the two centers, $N = P_2 - P_1$, is expected to correspond to Δϕ, we obtain a conversion factor c between pixel and angle $c = \Delta\phi/N$ [°/pixel], which can be used to obtain a relative angle relationship between pixels.

4.2.2.2. Obtain the conversion factor, c, via an accurate measurement of the distance between

the wafer surface and the sensor, and the pixel size (5.5*5.5µm for the sensor used here).

4.2.2.3. Estimate the absolute output angles in ϕ and θ for one of the CCD pixels. Set the beam center in θ to the expected emission angle according to simulations. In order to choose the absolute value in ϕ, optimize the beam for several angles in ϕ by adjusting the OPA phases, and record the intensity of the main lobe for each angle. According to the OPA theory, the main lobe is most intense (and the intensity in the side lobes minimized) when emitting at $\phi = 0°$. Hence, set the pixel in the center of the beam with the maximum recorded beam intensity, to $\phi = 0°$. Use this pixel and the conversion factor to assign absolute angles to all pixels of the image.

4.2.2.4. In the case of an output beam with significant tilt with respect to the vertical axis, and if the beam divergence and position must be measured very accurately, tilt the camera in order to be perfectly perpendicular to the output beam. Otherwise, it is also possible to apply a correction factor to the measured beam size by computing the projection of the beam on the sensor depending on the angle between the output beam and camera plane.

4.3. Calculation of the beam divergence

4.3.1. Extract cross sections across the center of the fundamental beam along ϕ and θ.

4.3.2. Fit two Gaussian curves to the cross sections and extract the full-width-at-half-maxima as a measure for the beam divergence ϕ_{div} and $\theta_{div.}$

4.3.3. Calculate the expected beam width $\phi_{div} = \lambda/Nd$ [°], where λ is the wavelength and d the lateral distance between the OPA gratings.

4.3.4. Estimate the beam divergence θ_{div} by performing FDTD simulations of the output gratings.

4.4. Automatic testing

4.4.1. If the characterization bench (as the one presented here) can perform automated measurements, perform some additional steps. First, obtain the chip dimensions and the coordinates of the measured structures from the circuit layout. Then, input those values to the bench control software. Therefore, once the input fiber have been aligned on the first tested structure (as detailed in section 2.1), the bench can switch automatically from one structure to another via a translation of the wafer.

REPRESENTATIVE RESULTS:

In this section, several in operando images of OPA beams are shown. These include images in the near and the far field of the beam, OPA output beams before and after phase optimization, and beams with a varying number of OPA channels.

An image of the near field of the beam, recorded using the microscope, can be seen in **Figure 5A**. The picture shows a passive OPA circuit with a large number of channels and the light emitted at the OPA gratings is clearly visible. This circuit produces an interference pattern in the far-field, which was recorded using the CCD sensor. The sensor image is given in **Figure 5B** and shows both the fundamental lobe as well as a side lobe. The exposure time of the sensor, the laser power and the background light have been optimized to produce a clear image. The two maxima are separated by 17.6°, calculated according to the equation given in the protocol section 4.2.2.1. Note that in this design, all waveguides are of the same length and therefore no significant phase difference between the channels is present. As a result, the interference maxima are clearly separated. An example of an OPA circuit with an irregular phase difference between the channels is presented below.

In order to observe clear interference maxima in the OPA output pattern, a linear phase difference between the OPA channels is required. However, when the length of the waveguides between the input and the output gratings varies from channel to channel, the interference pattern will show multiple, irregular interference sections along a straight line in the direction perpendicular to the grating orientation (i.e., along angle ϕ). An example of such an output pattern is given in the top left image of **Figure 6A**. It shows the far-field output of a 16-channel OPA with a non-uniform waveguide length between the input and output gratings. Fortunately, this OPA design has phase shifters included in every channel, so that the phases can be adjusted individually and the output beam shaped. After optimizing the phases as described in protocol section 3.3, the output beam forms one clear maximum. **Figure 6A** shows how the output beam evolves during the optimization process. Note that further interference maxima are present outside of the sensor area. In addition, we observe that the beam divergence of the 16-channels OPA is much broader than that seen in **Figure 5B**. This effect is expected and is due to a significant reduction in the channel number.

In the following, the operation of the optical circuit for OPA steering in two dimensions will be discussed, for details on the circuit see **Figure 2**. Firstly, the ring voltages of the switching network were calibrated in order to route the light to the different sub-circuits, each containing an OPA. Since the four OPAs each comprise a different grating period, routing the light between the sub-circuit results in the output beam being emitted at different θ angles. This is shown in **Figure 6B**, which contains the far-field images recorded as the light path is altered using the ring resonators of the switching network. The images show that the 'parallel' emission angle, θ, changes as each individual resonator is set on-resonance with the input light, while tuning the other resonators off-resonance. Our circuit was designed to access four different θ angles, however, due to a design error in the switching network, it was only possible to operate three of the ring resonators. From the output images, we can see that the interference pattern is irregular and no clear maxima are visible. In order to steer and shape the output beam in the 'perpendicular' emission angle, ϕ, the OPA phases were adjusted and optimized.

An example image of an optimized output beam of the two dimensional beam steering circuit is shown in **Figure 7A**. Two interference maxima are clearly visible, corresponding to the main lobe

and one of the side lobes. The top image in **Figure 7A** shows a heat map of the recorded brightness at the sensor versus pixel number. In order to determine the output angle, the image was processed as described in section 4.2 of the protocol and the relationship between pixel number and output angle determined. The calibrated image of beam intensity versus angle is shown in the bottom-most image of **Figure 7A**.

In the following, the beam steering results will be discussed. The OPA beam was successfully steered in an area of 17.6° × 3° (ϕ × θ), example data is shown in **Figure 7B and Figure 7C**. **Figure 7B** shows images of the beam being steered in ϕ while maintaining θ constant at 8°. This was achieved by first accessing the OPA corresponding to a parallel emission angle of θ = 8° and subsequently varying the optical phases to change the perpendicular emission angle, ϕ. Normalized intensity plots of the fundamental beam steered to three different output positions in θ are shown in **Figure 7C**, with a fixed perpendicular emission angle of ϕ = –2.5° and θ varying between 7° and 9°. As before, the parallel emission angle θ was controlled using the ring resonator network to switch between the OPAs. After OPA selection, the OPA phases were optimized to emit at ϕ = –2.5°.

Finally, the beam divergence was determined by fitting two Gaussian curves along ϕ and θ as described in protocol section 4.3. The FWHM serves as a measure for the beam divergence and was measured to be 4.3° in ϕ and 0.7° in θ for emission angles of ϕ = -2.5° and θ = 8°, see **Figure 8A**. These values are in good agreement with the expected values of 4.3° and 0.6° in ϕ and θ, respectively, for a four-channel OPA, as described in sections 4.3.3 and 4.3.4 of the protocol. In addition to determining the divergence of a four channel OPA, we investigated the divergence of an OPA design with a much larger number of channels. The divergence of a passive OPA consisting of 128 channels, with a design similar to that shown in **Figure 5A**, was measured. In order to test for fabrication variations across a wafer, we launched an automatic scan to characterize 42 devices with identical designs. The recorded images were analyzed with respect to the beam divergence. The divergence in ϕ versus position of the device on the wafer is shown in **Figure 8B**. The measured values lie between 0.19° and 0.37° and are slightly larger than the expected value of 0.14°. This could be explained by phase errors inside the individual OPA channels. All waveguides in the design are of the same length and therefore theoretically no phase differences should arise between the OPA channels. However, fabrication errors result in uncontrolled phase shifts as the light travels from the input to the output gratings, which leads to a broadening of the output beam. Due to the absence of phase shifters in the circuit, it was not possible to compensate for these errors. As mentioned, the θ angle is defined by the antenna grating geometry. Therefore, fabrication variations (SiN film height and structures lateral dimensions deviation) could affect the OPA output angle, θ. Such variations have been characterized on 40 devices across the whole wafer. Thanks to the very well controlled CMOS fabrication process, a negligible 3σ (three times the standard deviation) of 0.156° has been found.

FIGURE AND TABLE LEGENDS:

Figure 1: Illustration of integrated OPA. (**A**) The first-order interference lobe of the OPA output leaves the circuit at two azimuthal angles to the orthogonal projection of the chip plane, ϕ and

θ, perpendicular and parallel to the orientation of the grating respectively. (**B**) Top view of an OPA showing its main constitutive elements.

Figure 2: Schematic and microscope image of the integrated optical circuit for two dimensional beam steering. (**A**) Circuit containing a switching network connected to four sub-circuits, each forming an OPA. The output area contains four OPAs with four different grating periods and hence emission angles in θ. (**B**) Microscope image of the circuit described in (**A**), fabricated using SiN waveguides and Ti/TiN thermal phase shifters.

Figure 3: Electric circuit to apply electrical powers between 0 mW and 200 mW. This schematic represents an electric circuit which can individually apply voltages to the phase shifters in the optical circuit and read out their electrical current after voltage application. In our optical circuits, the phase shifters consist of electric wires with resistances of 1.3 kΩ. An electric power of 90 mW is required to achieve an optical phase shift of π. The circuit is controlled via an Arduino microcontroller.

Figure 4: Experimental set-up for OPA circuit characterization. (**A**) Schematic of the experimental set-up. (**B**) Picture of the experiment.

Figure 5: Near- and far field images of the output beam. (**A**) Near field image of an OPA circuit. Light at a wavelength of 905 nm is coupled into the circuit via a fiber and an input grating. Scattering of light inside the waveguides allows us to see the circuit design. At the end of an MMI tree, the light is emitted at the OPA gratings. (**B**) Far field image of the output of the circuit shown in (**A**). Two interference maxima are visible on the sensor. According to the OPA theory, the maxima are separated by 17.6°.

Figure 6: OPA beam optimization and switching network operation. (**A**) OPA beam optimization of a 16-channel OPA using phase shifters. Far-field images are shown after each optimization step. After optimising all 16 channels, the beam forms one main interference maximum inside the sensor area. (**B**) By using a switching network consisting of ring resonators, different OPAs each comprising a different grating period is accessed. The different grating periods result in the output beam emitting at different θ angles.

Figure 7: Characterization of the two dimensional beam steering circuit. (**A**) Pixel to angle conversion of the recorded image data. Beam steering results in ϕ and in θ are shown in (**B**) and (**C**), respectively. This figure has been modified from Tyler et al. [16]

Figure 8: OPA beam divergence measurements. (**A**) Beam divergence analysis of a 4-channel OPA. This figure has been modified from Tyler et al.[16] (**B**) Wafer map of measured divergences in ϕ of a 128 channel OPA design.

DISCUSSION:

We have presented a method to characterize an integrated OPA. The main advantage of the

method is the ability to easily probe multiple dies across a wafer, to look for fabrication variations and to identify high-performance devices. This can be seen in **Figure 8B**. From the wafer scan, it becomes clear that the lower half of the wafer exhibits devices with lower beam divergences. This could be explained by a higher waveguide quality in that area, which reduces random phase shifts and hence the beam divergence.

Using a large area CCD sensor to image the far field output is a convenient method to image the free space output of integrated circuits, since it can easily be added to most characterization set-ups due to their compact size in comparison to the often used, bulkier, Fourier-imaging systems[6].

In order to guarantee a high accuracy of the beam angle and divergence measurement, particular care must be taken during the camera – OPA alignment. Moreover, the OPA response is sensitive to phase and polarization instabilities during calibration. Therefore, all sources of perturbation must be controlled: movement/vibration of the injection fiber, laser temperature, incoming light polarization etc.

In summary, a method to characterize integrated OPAs was presented. Details on how to couple light, how to control phase shifters in the circuit and how to image the output in the near and the far field were given. Typical images of the output beams of several OPA circuits were shown, including the results of beam steering in two dimensions at a single wavelength in the near infrared. Furthermore, we show the results of measuring multiple devices with the same design across a wafer in terms of beam divergence. A performance trend with respect to the position on the wafer was found, identifying areas with high-quality fabrication properties.

ACKNOWLEDGMENTS:
This work was funded by the French Direction Générale des Entreprises (DGE) via the DEMO3S project.

DISCLOSURES:
The authors have nothing to disclose.

REFERENCES:

1. Heck, M. J. Highly integrated optical phased arrays: Photonic integrated circuits for optical beam shaping and beam steering. *Nanophotonics*. **6** (1), 93-107 (2017).
2. Vasey , F., Reinhart, F. K., Houdré, R., Stauffer, J. M. Spatial optical beam steering with an AlGaAs integrated phased array. *Applied Optics*. **32** (18), 3220-3232 (1993).
3. Van Acoleyen, K. et al. Off-chip beam steering with a one-dimensional optical phased array on silicon-on-insulator. *Optics Letters*. **34** (9), 1477-1479 (2009).
4. Guo, W. et al. Two dimensional optical beam steering with InP-based photonic integrated circuits. *IEEE Journal of Selected Topics in Quantum Electronics*. **19** (4), 6100212-6100212 (2013).
5. Jalali, B., Fathpour, S. Silicon photonics. *Journal of Lightwave Technology*. **24** (12), 4600-4615 (2006).
6. Hulme, J. C. Fully integrated hybrid silicon two dimensional beam scanner. *Optics Express*.

23 (5), 5861-5874 (2015).
7. Chung, S., Abediasl, H., Hashemi, H. A monolithically integrated large-scale optical phased array in silicon-on-insulator CMOS. *IEEE Journal of Solid-State Circuits*. **53** (1), 275-296 (2018).
8. Poulton, C. V. et al. Large-scale silicon nitride nanophotonic phased arrays at infrared and visible wavelengths. *Optics Letters*. **42** (1), 21-24 (2017).
9. Poulton, C. V. et al. Coherent solid-state LIDAR with silicon photonic optical phased arrays. *Optics Letters*. **42** (20), 4091-4094 (2017).
10. Martin, A. et al. Photonic integrated circuit based FMCW coherent LiDAR. *Journal of Lightwave Technology*. **36** (19), 4640 - 4645 (2018).
11. Subramanian, A. Z. et al. Low-Loss Single mode PECVD Silicon Nitride Photonic Wire Waveguides for 532–900 nm Wavelength Window Fabricated Within a CMOS Pilot Line. *IEEE Photonics Journal*. **5** (6), 2202809 (2013).
12. Baets, R. et al. Silicon Photonics: silicon nitride versus silicon-on-insulator. in *Optical Fiber Communication Conference, OSA Technical Digest (online) (Optical Society of America)*, paper Th3J.1 (2016).
13. Sabouri, S., Jamshidi, K. Design Considerations of Silicon Nitride Optical Phased Array for Visible Light Communications. *IEEE Journal of Selected Topics in Quantum Electronics*. **24** (6) (2018)
14. Zadka, M. et al. On-chip platform for a phased array with minimal beam divergence and wide field-of-view. *Optics Express*. **26** (3), 2528-2534 (2018).
15. Tyler, N. A. et al. SiN Integrated Photonics for near-infrared LIDAR. *2018 IEEE CPMT Symposium Japan (ICSJ)*. 63-66 (2018).
16. Tyler, N. A. et al. SiN integrated optical phased arrays for 2-dimensional beam steering at a single near-infrared wavelength. *Optics Express*. **27** (4), 5851-5858 (2019).

Figure

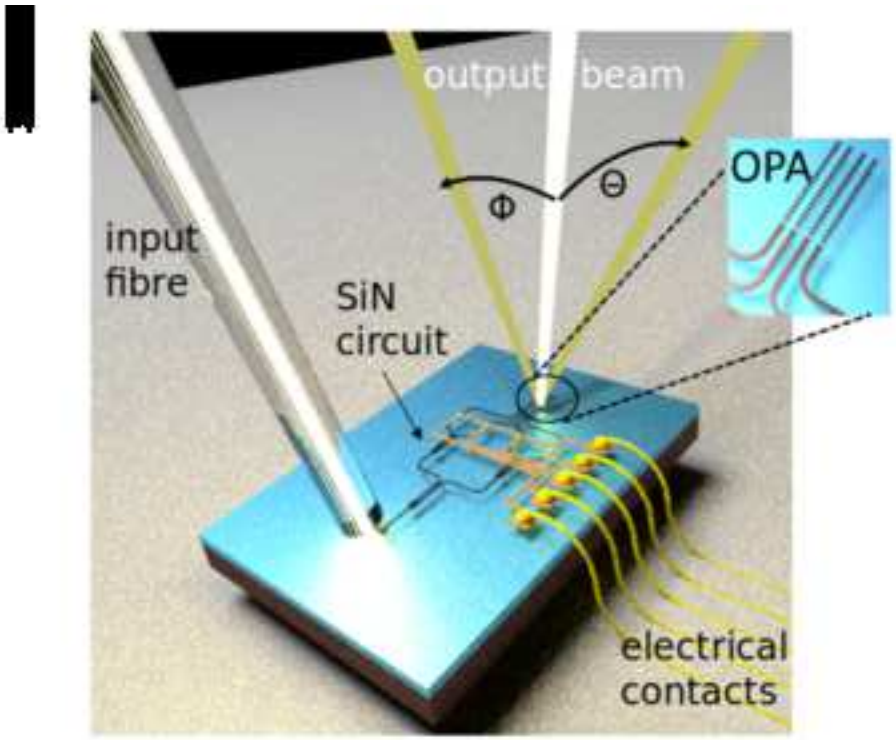

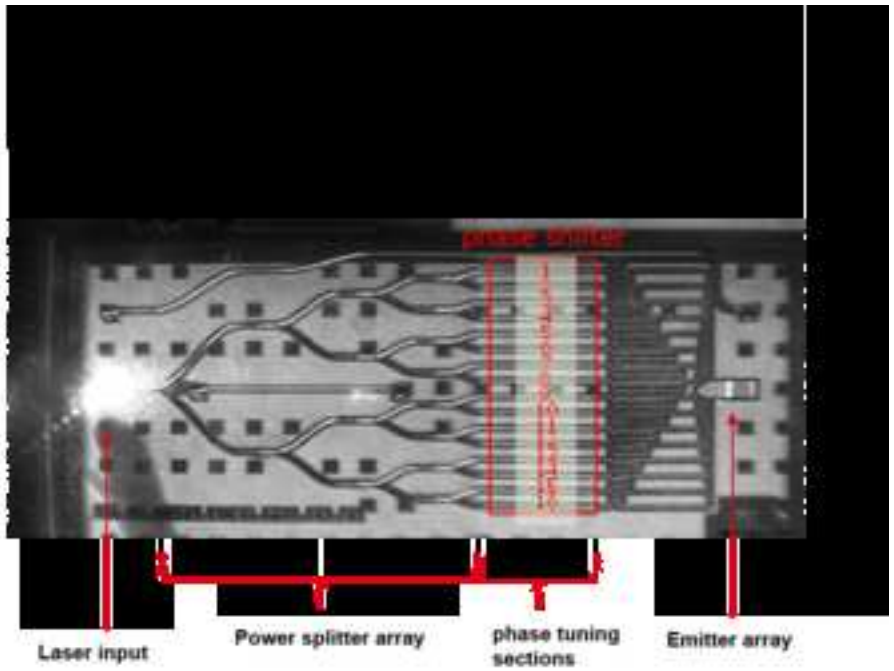

Figure

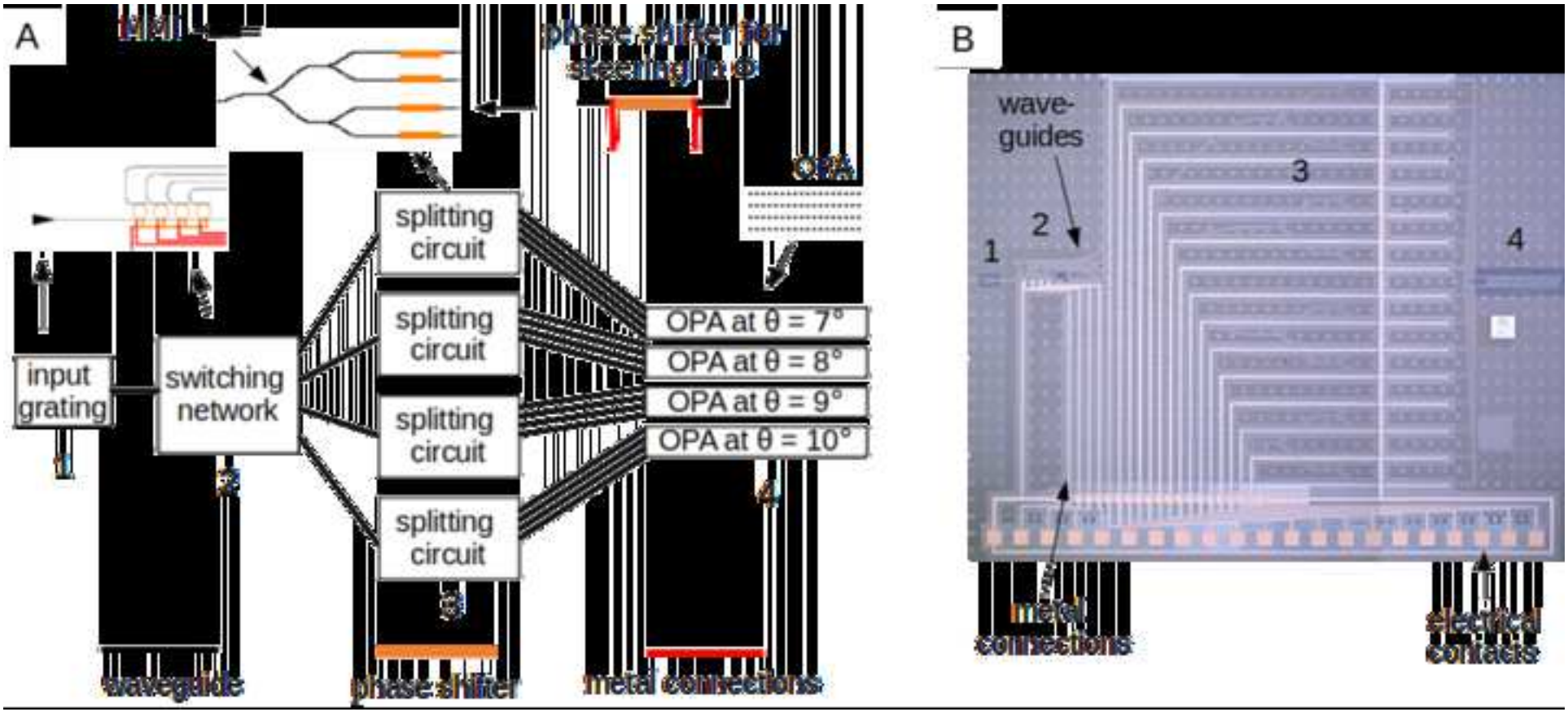

Figure

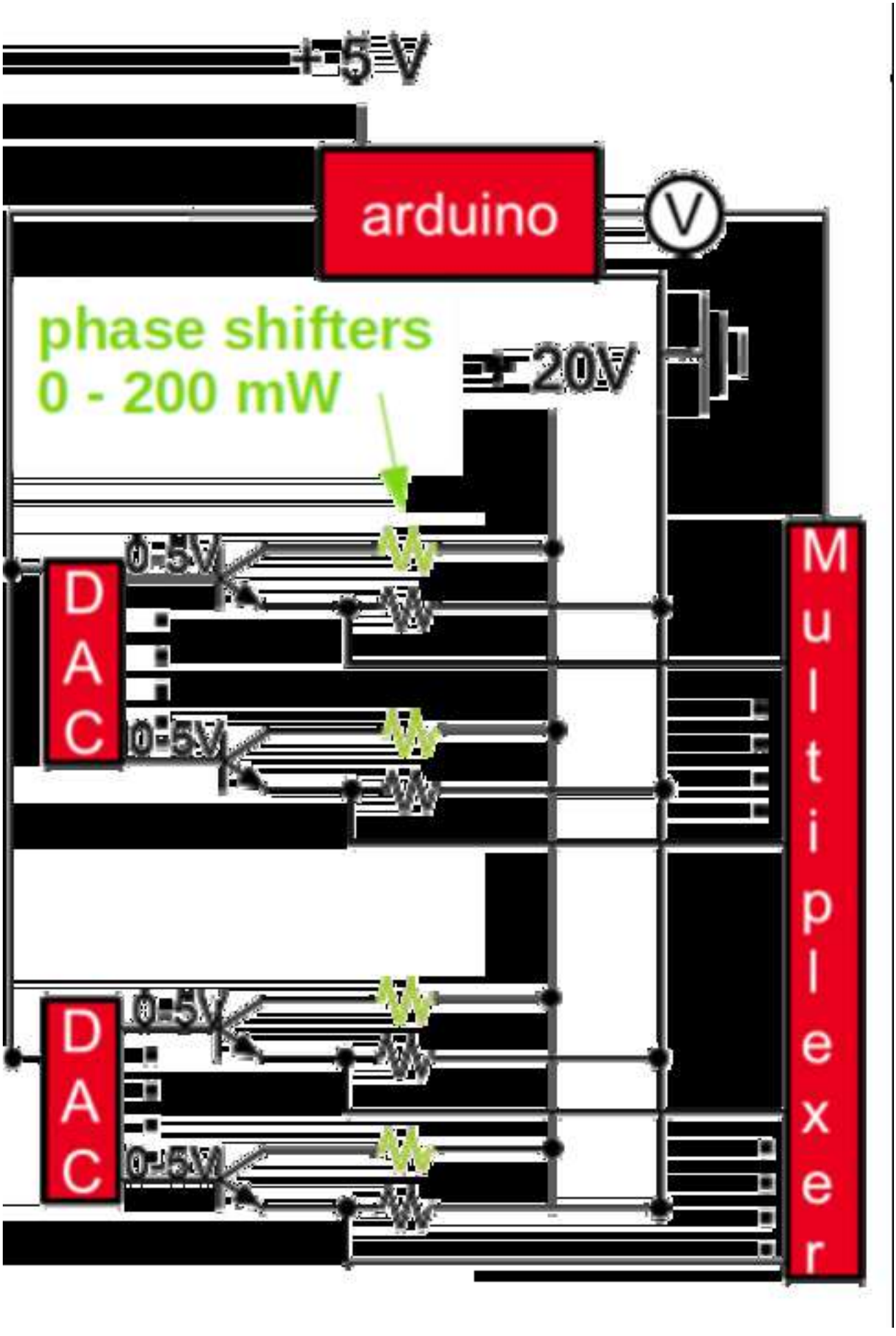

Figure

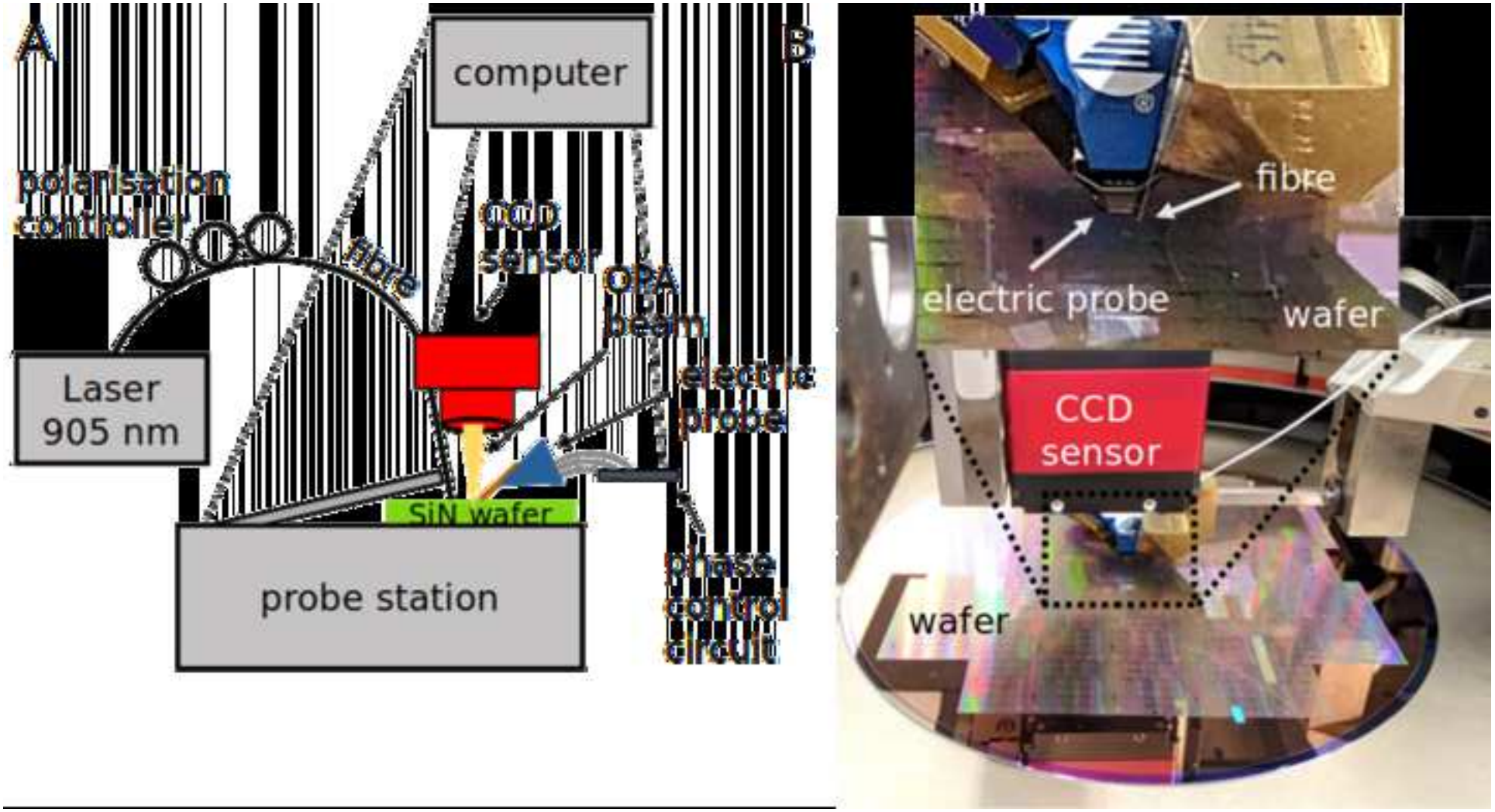

Figure

Click here to access/download;Figure;fig5_JOVE_Tyler_2019.psd

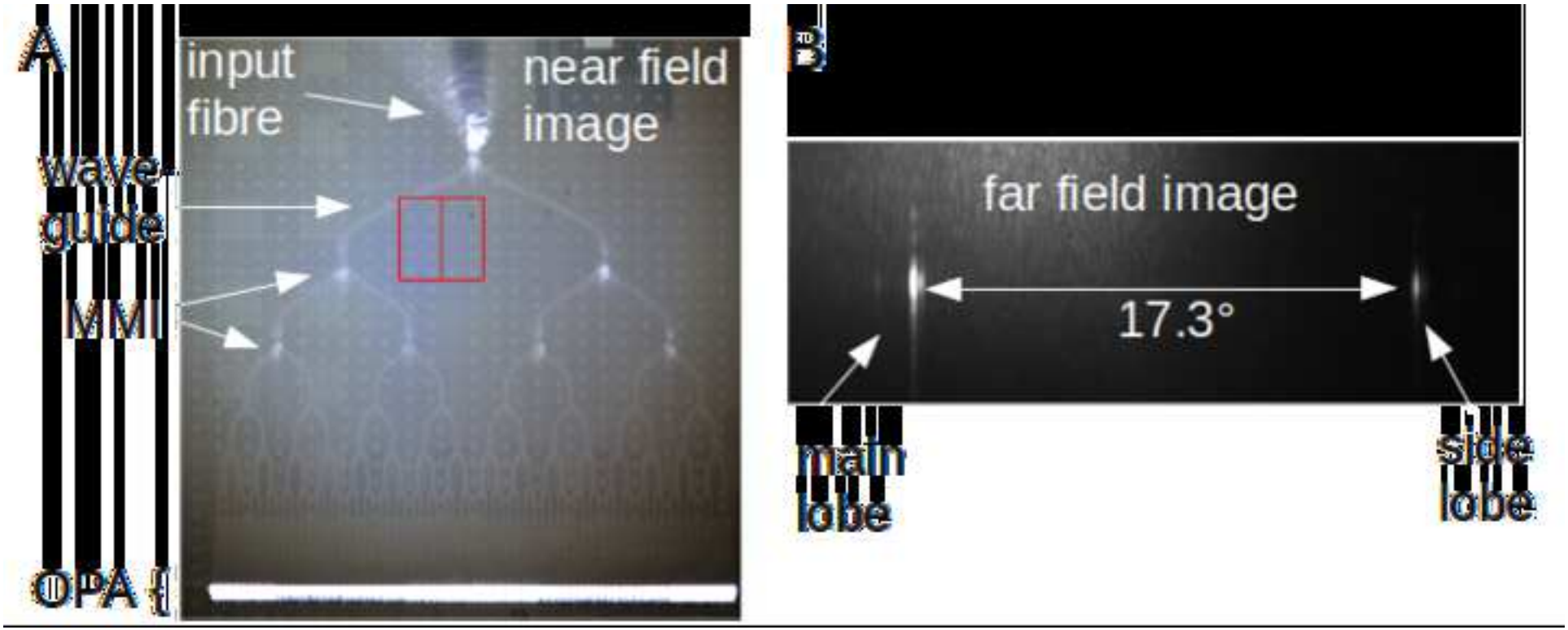

Figure

Click here to access/download;Figure;fig6_JOVE_Tyler_2019.psd

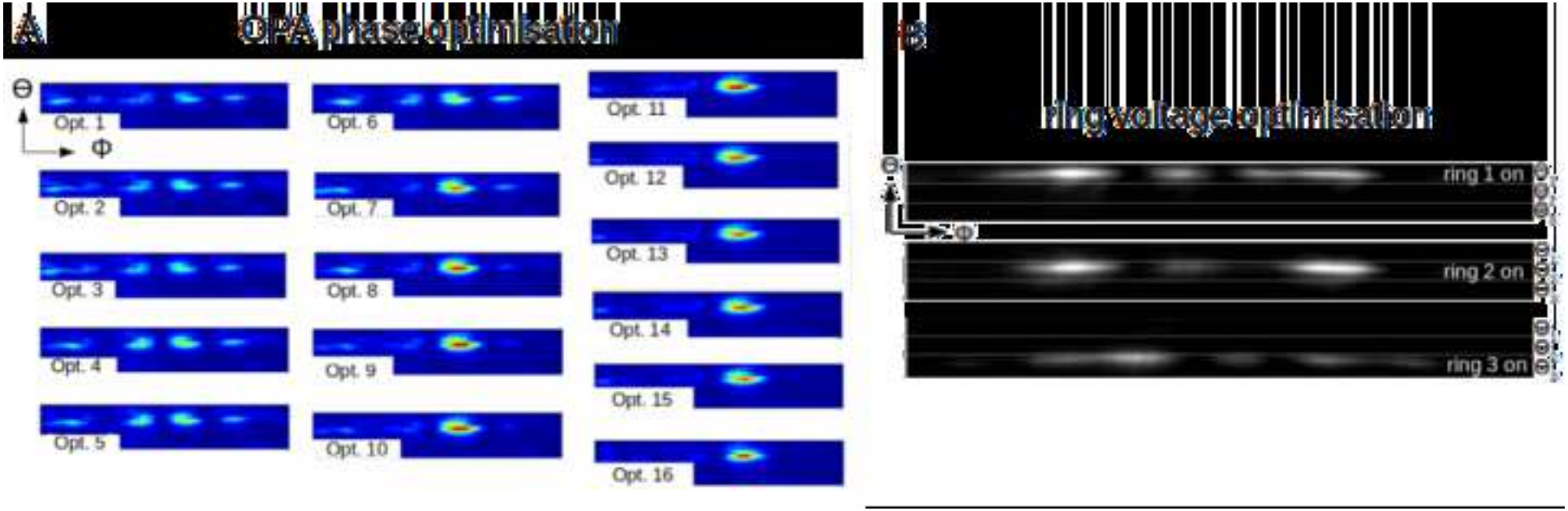

Figure

Click here to access/download;Figure;fig7_JOVE_Tyler_2019.psd

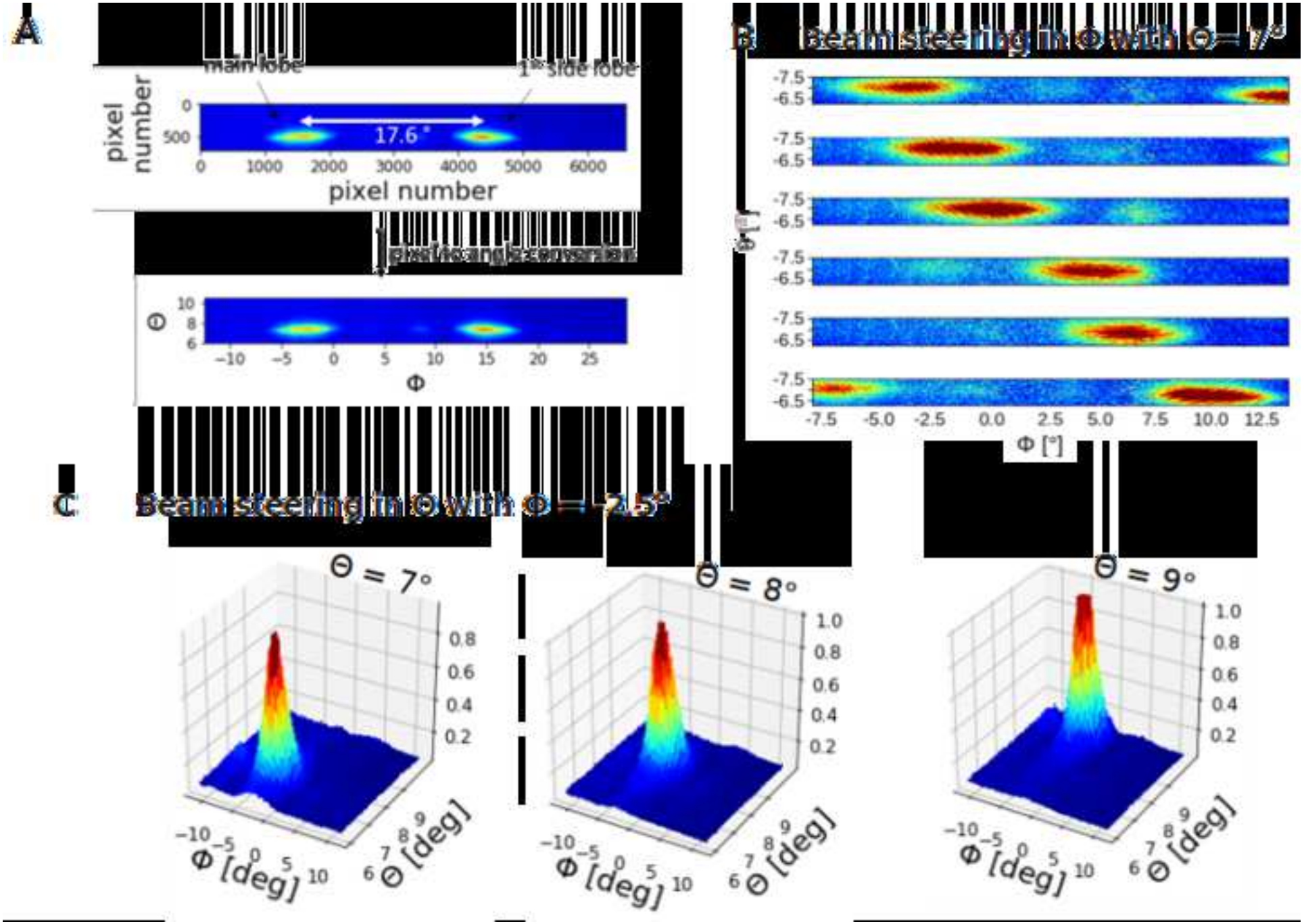

Figure

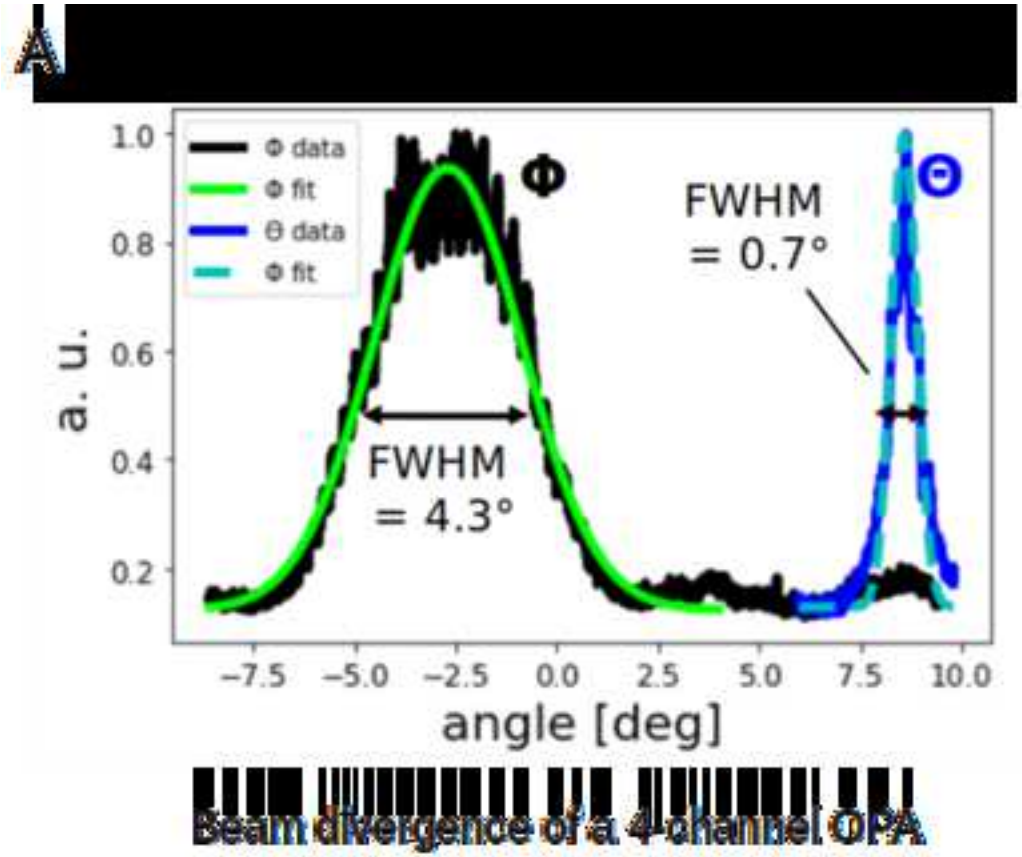

Beam divergence of a 4-channel OPA

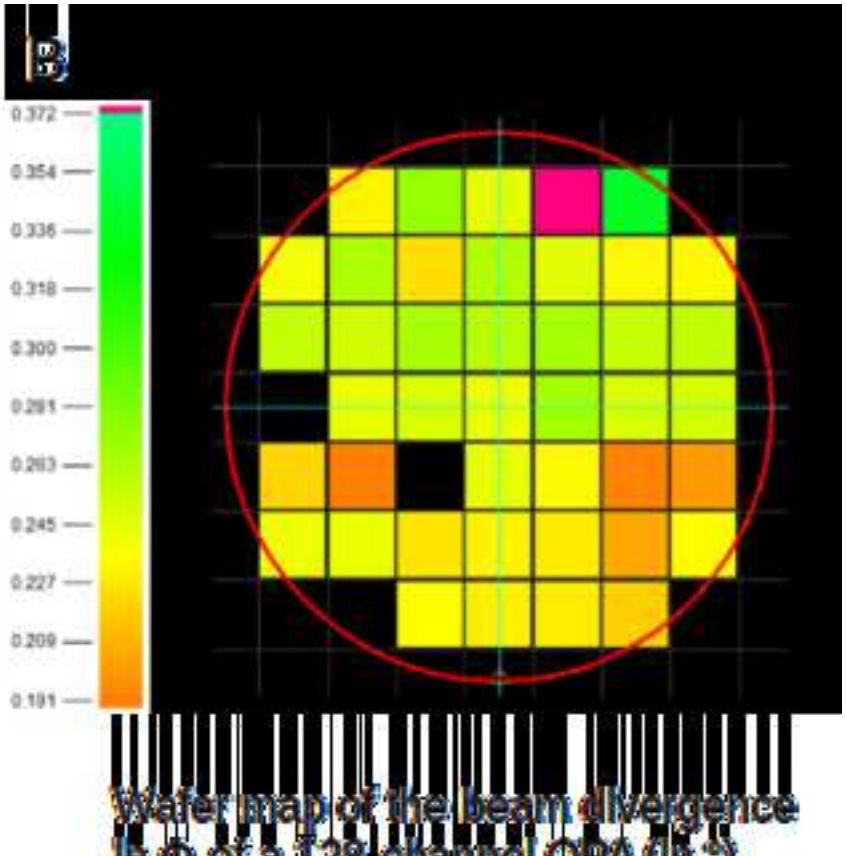

Wafer map of the beam divergence in Φ of a 128-channel OPA (in °)

Name of Material/Equipment	Company	Catalog Number	Comments/Description
25 ch electrical Probe	Cascade Microtech	InfinityQuad 25ch	
35 mm CCD sensor	Allied Vision	Prosilica GT 6600	
Arduino uno	Arduino	A100066	
laser	Qphotonics	QFLD-905-10S	
optical fibre	Corning	HI780	
polarization controller	ThorLabs	FPC023	
prober station	Cascade Microtech	Elite 300	

jove JOURNAL OF VISUALIZED EXPERIMENTS
1 Alewife Center #200
Cambridge, MA 02140
tel. 617.945.9051
www.jove.com

ARTICLE AND VIDEO LICENSE AGREEMENT

Title of Article: Characterization of SiN Integrated Optical Phased Arrays on a Wafer Scale Station Test

Author(s): Nicolas A Tyler, David Fowler, Stephane Malhouitre, Stephanie Garcia, Philippe Grosse, Wilfried Bahaud & Bertrand Szelag

Item 1: The Author elects to have the Materials be made available (as described at http://www.jove.com/publish) via:

☐ Standard Access ☑ Open Access

Item 2: Please select one of the following items:

☑ The Author is **NOT** a United States government employee.

☐ The Author is a United States government employee and the Materials were prepared in the course of his or her duties as a United States government employee.

☐ The Author is a United States government employee but the Materials were NOT prepared in the course of his or her duties as a United States government employee.

ARTICLE AND VIDEO LICENSE AGREEMENT

1. **Defined Terms.** As used in this Article and Video License Agreement, the following terms shall have the following meanings: "**Agreement**" means this Article and Video License Agreement; "**Article**" means the article specified on the last page of this Agreement, including any associated materials such as texts, figures, tables, artwork, abstracts, or summaries contained therein; "**Author**" means the author who is a signatory to this Agreement; "**Collective Work**" means a work, such as a periodical issue, anthology or encyclopedia, in which the Materials in their entirety in unmodified form, along with a number of other contributions, constituting separate and independent works in themselves, are assembled into a collective whole; "**CRC License**" means the Creative Commons Attribution-Non Commercial-No Derivs 3.0 Unported Agreement, the terms and conditions of which can be found at: http://creativecommons.org/licenses/by-nc-nd/3.0/legalcode; "**Derivative Work**" means a work based upon the Materials or upon the Materials and other pre-existing works, such as a translation, musical arrangement, dramatization, fictionalization, motion picture version, sound recording, art reproduction, abridgment, condensation, or any other form in which the Materials may be recast, transformed, or adapted; "**Institution**" means the institution, listed on the last page of this Agreement, by which the Author was employed at the time of the creation of the Materials; "**JoVE**" means MyJove Corporation, a Massachusetts corporation and the publisher of The Journal of Visualized Experiments; "**Materials**" means the Article and / or the Video; "**Parties**" means the Author and JoVE; "**Video**" means any video(s) made by the Author, alone or in conjunction with any other parties, or by JoVE or its affiliates or agents, individually or in collaboration with the Author or any other parties, incorporating all or any portion of the Article, and in which the Author may or may not appear.

2. **Background.** The Author, who is the author of the Article, in order to ensure the dissemination and protection of the Article, desires to have the JoVE publish the Article and create and transmit videos based on the Article. In furtherance of such goals, the Parties desire to memorialize in this Agreement the respective rights of each Party in and to the Article and the Video.

3. **Grant of Rights in Article.** In consideration of JoVE agreeing to publish the Article, the Author hereby grants to JoVE, subject to **Sections 4** and **7** below, the exclusive, royalty-free, perpetual (for the full term of copyright in the Article, including any extensions thereto) license (a) to publish, reproduce, distribute, display and store the Article in all forms, formats and media whether now known or hereafter developed (including without limitation in print, digital and electronic form) throughout the world, (b) to translate the Article into other languages, create adaptations, summaries or extracts of the Article or other Derivative Works (including, without limitation, the Video) or Collective Works based on all or any portion of the Article and exercise all of the rights set forth in (a) above in such translations, adaptations, summaries, extracts, Derivative Works or Collective Works and(c) to license others to do any or all of the above. The foregoing rights may be exercised in all media and formats, whether now known or hereafter devised, and include the right to make such modifications as are technically necessary to exercise the rights in other media and formats. If the "Open Access" box has been checked in **Item 1** above, JoVE and the Author hereby grant to the public all such rights in the Article as provided in, but subject to all limitations and requirements set forth in, the CRC License.

jove JOURNAL OF VISUALIZED EXPERIMENTS
1 Alewife Center #200
Cambridge, MA 02140
tel. 617.945.9051
www.jove.com

ARTICLE AND VIDEO LICENSE AGREEMENT

4. **Retention of Rights in Article.** Notwithstanding the exclusive license granted to JoVE in **Section 3** above, the Author shall, with respect to the Article, retain the non-exclusive right to use all or part of the Article for the non-commercial purpose of giving lectures, presentations or teaching classes, and to post a copy of the Article on the Institution's website or the Author's personal website, in each case provided that a link to the Article on the JoVE website is provided and notice of JoVE's copyright in the Article is included. All non-copyright intellectual property rights in and to the Article, such as patent rights, shall remain with the Author.

5. **Grant of Rights in Video – Standard Access.** This **Section 5** applies if the "Standard Access" box has been checked in **Item 1** above or if no box has been checked in **Item 1** above. In consideration of JoVE agreeing to produce, display or otherwise assist with the Video, the Author hereby acknowledges and agrees that, Subject to **Section 7** below, JoVE is and shall be the sole and exclusive owner of all rights of any nature, including, without limitation, all copyrights, in and to the Video. To the extent that, by law, the Author is deemed, now or at any time in the future, to have any rights of any nature in or to the Video, the Author hereby disclaims all such rights and transfers all such rights to JoVE.

6. **Grant of Rights in Video – Open Access.** This **Section 6** applies only if the "Open Access" box has been checked in **Item 1** above. In consideration of JoVE agreeing to produce, display or otherwise assist with the Video, the Author hereby grants to JoVE, subject to **Section 7** below, the exclusive, royalty-free, perpetual (for the full term of copyright in the Article, including any extensions thereto) license (a) to publish, reproduce, distribute, display and store the Video in all forms, formats and media whether now known or hereafter developed (including without limitation in print, digital and electronic form) throughout the world, (b) to translate the Video into other languages, create adaptations, summaries or extracts of the Video or other Derivative Works or Collective Works based on all or any portion of the Video and exercise all of the rights set forth in (a) above in such translations, adaptations, summaries, extracts, Derivative Works or Collective Works and (c) to license others to do any or all of the above. The foregoing rights may be exercised in all media and formats, whether now known or hereafter devised, and include the right to make such modifications as are technically necessary to exercise the rights in other media and formats. For any Video to which this **Section 6** is applicable, JoVE and the Author hereby grant to the public all such rights in the Video as provided in, but subject to all limitations and requirements set forth in, the CRC License.

7. **Government Employees.** If the Author is a United States government employee and the Article was prepared in the course of his or her duties as a United States government employee, as indicated in **Item 2** above, and any of the licenses or grants granted by the Author hereunder exceed the scope of the 17 U.S.C. 403, then the rights granted hereunder shall be limited to the maximum rights permitted under such statute. In such case, all provisions contained herein that are not in conflict with such statute shall remain in full force and effect, and all provisions contained herein that do so conflict shall be deemed to be amended so as to provide to JoVE the maximum rights permissible within such statute.

8. **Protection of the Work.** The Author(s) authorize JoVE to take steps in the Author(s) name and on their behalf if JoVE believes some third party could be infringing or might infringe the copyright of either the Author's Article and/or Video.

9. **Likeness, Privacy, Personality.** The Author hereby grants JoVE the right to use the Author's name, voice, likeness, picture, photograph, image, biography and performance in any way, commercial or otherwise, in connection with the Materials and the sale, promotion and distribution thereof. The Author hereby waives any and all rights he or she may have, relating to his or her appearance in the Video or otherwise relating to the Materials, under all applicable privacy, likeness, personality or similar laws.

10. **Author Warranties.** The Author represents and warrants that the Article is original, that it has not been published, that the copyright interest is owned by the Author (or, if more than one author is listed at the beginning of this Agreement, by such authors collectively) and has not been assigned, licensed, or otherwise transferred to any other party. The Author represents and warrants that the author(s) listed at the top of this Agreement are the only authors of the Materials. If more than one author is listed at the top of this Agreement and if any such author has not entered into a separate Article and Video License Agreement with JoVE relating to the Materials, the Author represents and warrants that the Author has been authorized by each of the other such authors to execute this Agreement on his or her behalf and to bind him or her with respect to the terms of this Agreement as if each of them had been a party hereto as an Author. The Author warrants that the use, reproduction, distribution, public or private performance or display, and/or modification of all or any portion of the Materials does not and will not violate, infringe and/or misappropriate the patent, trademark, intellectual property or other rights of any third party. The Author represents and warrants that it has and will continue to comply with all government, institutional and other regulations, including, without limitation all institutional, laboratory, hospital, ethical, human and animal treatment, privacy, and all other rules, regulations, laws, procedures or guidelines, applicable to the Materials, and that all research involving human and animal subjects has been approved by the Author's relevant institutional review board.

11. **JoVE Discretion.** If the Author requests the assistance of JoVE in producing the Video in the Author's facility, the Author shall ensure that the presence of JoVE employees, agents or independent contractors is in accordance with the relevant regulations of the Author's institution. If more than one author is listed at the beginning of this Agreement, JoVE may, in its sole

jove JOURNAL OF VISUALIZED EXPERIMENTS
1 Alewife Center #200
Cambridge, MA 02140
tel. 617.945.9051
www.jove.com

ARTICLE AND VIDEO LICENSE AGREEMENT

discretion, elect not take any action with respect to the Article until such time as it has received complete, executed Article and Video License Agreements from each such author. JoVE reserves the right, in its absolute and sole discretion and without giving any reason therefore, to accept or decline any work submitted to JoVE. JoVE and its employees, agents and independent contractors shall have full, unfettered access to the facilities of the Author or of the Author's institution as necessary to make the Video, whether actually published or not. JoVE has sole discretion as to the method of making and publishing the Materials, including, without limitation, to all decisions regarding editing, lighting, filming, timing of publication, if any, length, quality, content and the like.

12. **Indemnification.** The Author agrees to indemnify JoVE and/or its successors and assigns from and against any and all claims, costs, and expenses, including attorney's fees, arising out of any breach of any warranty or other representations contained herein. The Author further agrees to indemnify and hold harmless JoVE from and against any and all claims, costs, and expenses, including attorney's fees, resulting from the breach by the Author of any representation or warranty contained herein or from allegations or instances of violation of intellectual property rights, damage to the Author's or the Author's institution's facilities, fraud, libel, defamation, research, equipment, experiments, property damage, personal injury, violations of institutional, laboratory, hospital, ethical, human and animal treatment, privacy or other rules, regulations, laws, procedures or guidelines, liabilities and other losses or damages related in any way to the submission of work to JoVE, making of videos by JoVE, or publication in JoVE or elsewhere by JoVE. The Author shall be responsible for, and shall hold JoVE harmless from, damages caused by lack of sterilization, lack of cleanliness or by contamination due to the making of a video by JoVE its employees, agents or independent contractors. All sterilization, cleanliness or decontamination procedures shall be solely the responsibility of the Author and shall be undertaken at the Author's expense. All indemnifications provided herein shall include JoVE's attorney's fees and costs related to said losses or damages. Such indemnification and holding harmless shall include such losses or damages incurred by, or in connection with, acts or omissions of JoVE, its employees, agents or independent contractors.

13. **Fees.** To cover the cost incurred for publication, JoVE must receive payment before production and publication of the Materials. Payment is due in 21 days of invoice. Should the Materials not be published due to an editorial or production decision, these funds will be returned to the Author. Withdrawal by the Author of any submitted Materials after final peer review approval will result in a US$1,200 fee to cover pre-production expenses incurred by JoVE. If payment is not received by the completion of filming, production and publication of the Materials will be suspended until payment is received.

14. **Transfer, Governing Law.** This Agreement may be assigned by JoVE and shall inure to the benefits of any of JoVE's successors and assignees. This Agreement shall be governed and construed by the internal laws of the Commonwealth of Massachusetts without giving effect to any conflict of law provision thereunder. This Agreement may be executed in counterparts, each of which shall be deemed an original, but all of which together shall be deemed to me one and the same agreement. A signed copy of this Agreement delivered by facsimile, e-mail or other means of electronic transmission shall be deemed to have the same legal effect as delivery of an original signed copy of this Agreement.

A signed copy of this document must be sent with all new submissions. Only one Agreement is required per submission.

CORRESPONDING AUTHOR

Name:	DAVID FOWLER
Department:	DOPT / SNAP / LP2C
Institution:	CEA - LETI
Title:	RESEARCH ENGINEER
Signature:	
Date:	10/05/2019

Please submit a **signed** and **dated** copy of this license by one of the following three methods:

1. Upload an electronic version on the JoVE submission site
2. Fax the document to +1.866.381.2236
3. Mail the document to JoVE / Attn: JoVE Editorial / 1 Alewife Center #200 / Cambridge, MA 02140

Dear Dr. Fowler,

Your manuscript, JoVE60269 "Characterization of SiN integrated optical phased arrays on a wafer-scale test station," has been editorially and peer reviewed, and the following comments need to be addressed. Note that editorial comments address both requirements for video production and formatting of the article for publication. Please track the changes within the manuscript to identify all of the edits.

After revising and uploading your submission, please also upload a separate rebuttal document that addresses each of the editorial and peer review comments individually. Please submit each figure as a vector image file to ensure high resolution throughout production: (.psd, ai, .eps., .svg). Please ensure that the image is 1920 x 1080 pixels or 300 dpi. Additionally, please upload tables as .xlsx files.

Your revision is due by **Jul 17, 2019**.

To submit a revision, go to the JoVE submission site and log in as an author. You will find your submission under the heading "Submission Needing Revision". Please note that the corresponding author in Editorial Manager refers to the point of contact during the review and production of the video article.

Best,

Bing Wu, Ph.D.
Review Editor
JoVE

Editorial comments:

1. Please take this opportunity to thoroughly proofread the manuscript to ensure that there are no spelling or grammar issues.
2. Please obtain explicit copyright permission to reuse any figures from a previous publication. Explicit permission can be expressed in the form of a letter from the editor or a link to the editorial policy that allows re-prints. Please upload this information as a .doc or .docx file to your Editorial Manager account. The Figure must be cited appropriately in the Figure Legend, i.e. “This figure has been modified from [citation].”
3. Please ensure that all text in the protocol section is written in the imperative tense as if telling someone how to do the technique (e.g., “Do this,” “Ensure that,” etc.). Any text that cannot be written in the imperative tense may be added as a “Note.”
4. Please revise the text in Protocol to avoid the use of any personal pronouns (e.g., "we", "you", "our" etc.).
5. Please add a one-line space between each of your protocol steps.
6. There is a 2.75 page limit for filmable content. Please highlight 2.75 pages or less of the Protocol steps (including headings and spacing) in yellow that identifies the essential steps of the protocol for the video, i.e., the steps that should be visualized to tell the most cohesive

story of the Protocol.
7. Please revise the Discussion to explicitly cover the following in detail in 3-6 paragraphs with citations:
a) Critical steps within the protocol
b) Any modifications and troubleshooting of the technique
c) Any limitations of the technique
d) The significance with respect to existing methods
e) Any future applications of the technique
8. Please do not abbreviate journal titles for references.
9. Please remove the embedded figure(s) from the manuscript. All figures should be uploaded separately to your Editorial Manager account.

Reviewers' comments:
Reviewer #1:
Manuscript Summary:
The authors developed and presented a protocol for a wafer level characterization of the they propose optical phased array on SiN platform. The protocol is clearly presented and wafer level characterization results are shown. I recommend to accept this paper in its current form.

Major Concerns:
None.

Minor Concerns:
(1) The divergence angle θ variation across the wafer would also be of interest to indicate the grating strength variation (due to the duty cycle change, waveguide width change, SiN thickness change and etc). The authors should also discuss this result based on our measurement.
=> Two kind of variations may affect the antenna behavior. Firstly, the SiN height could vary during the deposition. Secondly, the structures lateral dimensions may differ from the design due to imperfections during the lithography and patterning steps. However, thanks to the well-known CMOS fabrication environment, such variations are extremely small. As suggested, the θ variation have been characterised on 40 dies across the wafer. A 3σ of 0.156° has been found, confirming the relatively small impact of the aforementioned variations on the antenna.
Details have been added in the representative results part.

(2) Switching between the CCD and optical microscope might not be easy. The author could discuss a better way or more cost-effective way to shift between Farfield imaging and nearfield imaging for alignment optimization.
=> A paragraph (1.1.7) about this has been added.

(3) Laser power level might need to be adjusted to avoid saturate the image and get good SNR. The author should also discuss this in their protocol.
=> Indeed, in order to avoid image saturation the laser power must be adjusted to the camera integration time. This is discussed in section 2.2. OPA output imaging

Reviewer #2:

Manuscript Summary:
This manuscript summarizes a protocol for measuring the beam steering angle and beam divergence for integrated photonic phased arrays. The authors summarize a photonic device that they have published elsewhere and describe, in detail, the method that they used to characterize the device. They provide good background on the device and also fill in a number of the details of the characterization method that are hard to find in the literature more generally.

Major Concerns:
1. There is little to no introduction and background on the method that they are presenting, and there is no attempt made to compare and contrast it to other available methods (for example, imaging systems, imaging the array output on a screen or wall, etc..) nor to explain why (or when) it is superior. The introduction focuses on introducing their device and the concept of phased arrays instead of focusing on the various characterization methods for optical phased arrays. Details like the cross-section of their device, its performance, and the chip fabrication should be replaced by details explaining and motivating the characterization method.
=> Details about the presented characterization method have been added in the Introduction section. The choice of a bare image sensor placed on top of the OPA has been justified as well as briefly compared with other possible OPA output far field characterization setups.

2. An important part of the method is in section 4 where the CCD pixels are correlated to the output angles. The authors make two key assumptions here without providing sufficient justification: 1. They assume that this calibration will be the same in both directions - something that will not be true if there is significant tilt on the imager with respect to the chip output (that is if the plane of the imager is not perpendicular to the output beam), and 2. They assume a match between their simulation and experiment and use the simulation result to calibrate the image, thus making it impossible to measure a difference between theory and experiment. More justification for these two steps needs to be added.
=> 1. A paragraph (4.2.2.4) have been added describing a specific procedure for the case of a strongly tilted output beam.
2. The match that we are assuming is between experiment and an analytical formula (not a simulation) that is exact. Moreover, the distance between the antennas (that is in the order of µm) is very accurately controlled since they are defined by DUV lithography. Therefore we are able to perform an accurate calibration of the conversion factor between pixels and beam shape (angle and size). However, another method has been proposed (4.2.2.2.) to obtain the conversion factor using only measurement and trigonometry and not the aforementioned analytical formula and any assumption about the antennas pitch.

3. Similarly, the "representative results" section focuses too narrowly on describing the performance of their device and needs a more general description of the various results that could be seen and what they might mean. The goal here is to help the experimenter understand what they are seeing, not present the performance of the device the authors developed and previously published.
=> Some additional explanations have been added.

4. The authors hint at the ability to do wafer level testing, but this is not described in sufficient

detail to be useful to the reader. They mention that they do an automatic scan, but do not explain how it is set up. There is no mention of wafer level testing in the "Protocol" section at all. Instead, it is described in the last paragraph of "Representative results". This should either be included in the protocol or cut.
=> A paragraph (4.4) have been added in the protocol section.

5. The figures need to be cleaned up: higher resolution is needed for the images, along with clearer labeling and general clean up.
=> Figures have been updated.

Minor Concerns:
1. The authors go out of their way to motivate the use of silicon nitride over silicon in their device. This is immaterial to their characterization method (variants of which could work for either) and so feels out of place. Also, the authors claim that there are no non-linear losses in SiN is un-true; such losses just become important at higher powers than in silicon.
=> This is only detailed over a few lines to give a bit of context and information about the characterized device and also to justify the operating wavelength. Regarding the nonlinear losses of SiN, I agree that our explanation was a bit confusing. Of course nonlinear optical losses can take place in SiN, however it's at a significantly higher power level than that which is currently proposed for use in LiDAR. This have been reformulated in the article.

2. More detail on the control circuit described in 1.1.5 would be useful. Similarly, a bit more detail on the mounting and control system in section 1.2.1 would be useful.
=> Some details describing the electrical control circuit and the control system have been added.

3. More information on how to trouble shoot if things aren't working would be helpful throughout. For example, in section 2.1.1., what should the experimenter do if they do not see light exiting the OPA output gratings.
=> Information have been added in section 2.1.2.

4. The order of images in figure 6 should be switched to follow the order they are referenced in the text (6B then 6A).
=> To me the order is right, figure 6A (line 314) is mentioned before figure 6B (line 328).

5. How many channels are used to generate the image in 5b?
=> It's a 128ch OPA. This information has been added.

6. An accompanying cartoon would be helpful for figure 1.
=> A picture detailing the OPA circuit has been added.